Proceedings of ASME Turbo Expo 2019: Turbomachinery Technical Conference and Exposition
SAND2019-1768C
GT2019
June 17-21, 2019, Phoenix, Arizona, USA

GT2019-91772

COMPACT HEAT EXCHANGER SEMI-CIRCULAR HEADER BURST PRESSURE AND STRAIN VALIDATION

Blake W. Lance
Sandia National Laboratories
Albuquerque, NM, USA

Matthew D. Carlson
Sandia National Laboratories
Albuquerque, NM, USA

ABSTRACT

Compact heat exchangers for supercritical CO_2 (sCO_2) service are often designed with external, semi-circular headers. Their design is governed by the ASME Boiler & Pressure Vessel Code (BPVC) whose equations were typically derived by following Castigliano's Theorems. However, there are no known validation experiments to support their claims of pressure rating or burst pressure predictions nor is there much information about how and where failures occur.

This work includes high pressure bursting of three semi-circular header prototypes for the validation of three aspects: (1) burst pressure predictions from the BPVC, (2) strain predictions from Finite Element Analysis (FEA), and (3) deformation from FEA. The header prototypes were designed with geometry and weld specifications from the BPVC Section VIII Division 1, a design pressure typical of sCO_2 service of 3,900 psi (26.9 MPa), and were built with 316 SS. Repeating the test in triplicate allows for greater confidence in the experimental results and enables data averaging. Burst pressure predictions are compared with experimental results for accuracy assessment. The prototypes are analyzed to understand their failure mechanism and locations.

Experimental strain and deformation measurements were obtained optically with Digital Image Correlation (DIC). This technique allows strain to be measured in two dimensions and even allows for deformation measurements, all without contacting the prototype. Eight cameras are used for full coverage of both headers on the prototypes. The rich data from this technique are an excellent validation source for FEA strain and deformation predictions. Experimental data and simulation predictions are compared to assess simulation accuracy.

INTRODUCTION

Compact, diffusion bonded heat exchangers are a critical technology for supercritical sCO_2 power cycles because they have a design well suited for high pressures and are smaller and less expensive than standard shell and tube designs for these pressures. These heat exchangers require headers to direct the flow from a connected nozzle and distribute it to typically thousands of microchannels. The most common header design is the external, semi-circular header as shown in Figure 1. These headers are welded onto the diffusion bonded core.

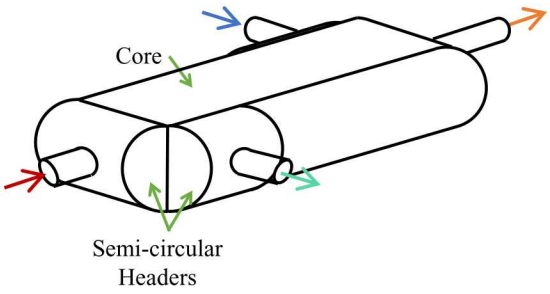

Figure 1, Compact heat exchanger sketch with semi-circular headers

Compact heat exchanger vendors often design to the requirements of the ASME BPVC, Section VIII, Division 1 [1] and provide an ASME U-stamp of their products as pressure vessels. This standard uses 'design by equation' to define the pressure vessel geometry given the desired pressure rating, the allowable material stress from the BPVC, Section II, Part D, and the weld joint efficiency. The governing equations derived for elastic strain energy and Castigliano's theorems are used in at least one publication [2] whose figures are repeated with striking similarity in the BPVC. This similarity suggests that the design equations in the BPVC are theoretically based and not empirical. These are in Mandatory Appendix 13 for Vessels of Noncircular Cross Section. According to section 13-2, this appendix also covers "vessels of circular section with a single diametral plate" as shown in Figure 2 [1].

Castigliano's theorems were initially written in French in 1879 and have seen utilization since that time [3]. In 1923, Southwell provided some discussion on this theorem, this time written in English [4]. His restatement is:

> In a framework which is not initially self-strained, the stresses imposed by a given system of external forces may be found from the conditions for a minimum value of the total strain-energy, if account be taken of the conditions of equilibrium.

Perhaps even more simply stated, the material will elastically deform in a way that minimizes the total strain energy. This is the basis for Faupel's derivations of stress predictions in a wide range of rectangular pressure vessel designs that form much of

Sandia National Laboratories is a multimission laboratory managed and operated by National Technology & Engineering Solutions of Sandia, LLC, a wholly owned subsidiary of Honeywell International Inc., for the U.S. Department of Energy's National Nuclear Security Administration under contract DE-NA0003525.

the BPVC [2], [1], likely including the circular pressure vessel with a single stay plate.

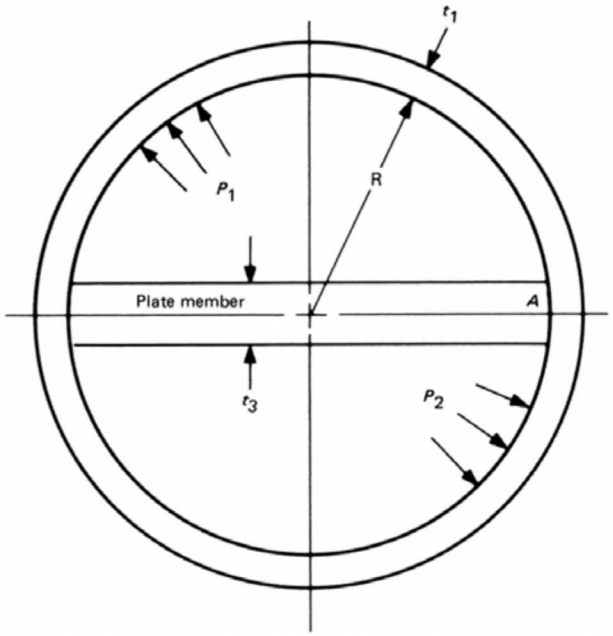

Figure 2, Vessel of circular cross section with diametral stay plate, from [1]

Even though the elastic strain energy theorem has been used for over 100 years and has been adopted as the basis for the BPVC, there is no known experimental validation for its use in semi-circular headers for compact heat exchangers. To this end, this work seeks to provide experimental validation to the BPVC for this geometry on the basis of burst pressure predictions. In addition, optical strain measurements of burst experiments with DIC provide a rich dataset and a potential validation data source for FEA predictions.

SEMI-CIRCULAR HEADER DESIGN EQUATIONS

Stress Predictions in Shells and Stays

Semi-circular headers can be designed using the ASME BPVC 'design by equation' guidance found in Section VIII, Division 1, Mandatory Appendix 13, section 13 for "Vessels of Circular Cross Section Having a Single Diametral Staying Member" as sketched in Figure 2. In this case, the diffusion bonded core can be interpreted as an overly thick stay plate. Subsection 13-13(b) applies to pressure vessels with equal pressures in both compartments. This is a reasonable assumption for sCO_2 heat exchangers as the gauge pressure is generally 70-300 bar and the pressure drop across the heat exchangers is often around 1-3 bar.

The semi-circular header is termed the 'shell section' and the core is termed the 'diametral plate'. The total stress in the shell is the sum of the membrane stress from a pressure differential across its faces and bending stress from elastic deformation with constrained ends. It is calculated by Equation (1) where the total stress is a sum of two terms; the first term being the membrane stress and the second term being the bending stress.

$$S_{T,\text{shell}} = \frac{PR}{t_{\text{shell}}} + \frac{c}{I}\left[\frac{2Pt_{\text{shell}}^2}{3(\pi^2-8)}\right] \tag{1}$$

In the plate, the total stress is purely a membrane stress because there is no appreciable pressure difference across its faces. It is defined by

$$S_{T,\text{plate}} = \frac{2\pi P t_{\text{shell}}^2}{3Rt_{plate}(\pi^2-8)} \tag{2}$$

where, for both equations, P is the internal pressure, R is the inside radius, t_{shell} is the shell thickness, $I = bt^3/12$ is the moment of inertia on a per-unit-width basis with $b = 1.0$, and t_{plate} is the plate thickness. The variable c is the distance to the neutral axis, is defined in 13-4(c), and changes sign depending on whether the shell is in tension (positive) or compression (negative). Since we are only considering internal pressure, the maximum total stress will occur in the inner layer of the shell when in tension, so $c = t_{\text{shell}}/2$. The code also states in 13-13(a) that "Stresses need to be computed only at the shell-plate junction since this is the location of maximum stress" [1].

Design Requirements in Shells, Stays, and End Caps

The shell has two design rules for stress that need to be considered for the thickness requirement as outlined in subsection 13-4(b). For welded headers, the first limit is that the membrane stress at a weld joint shall not exceed SE where S is the allowable stress from BPVC Section II, Part D and E is the weld joint efficiency. The weld joint efficiency varies from 0.7 to 1.0 for butt joints, with increasing values for higher levels of weld inspection, according to Table UW-12. Simply stated, an efficiency of 1.0 is used for full radiographic examination, 0.85 for spot examination, and 0.70 for no examination. The second limit is that the total stress shall not exceed the lesser of $1.5SE$ or $2/3$ of the yield strength S_y of the material at design temperature. The second rule only applies to the shell as the plate will not be subject to bending stresses since the pressures are assumed equal on both sides. The total (membrane only) stress in the stay plate shall not exceed SE.

Applying the above rules and substitutions to Equation (1) for the shell provides two equations that can define the thickness based on the two rules,

$$S_{\text{membrane,shell}} = \frac{PR}{t_{\text{shell}}} \le SE, \qquad t_{\text{shell}} \ge \frac{PR}{SE} \tag{3}$$

and

$$S_{T,\text{shell}} = \frac{PR}{t_{\text{shell}}} + \frac{4P}{\pi^2-8} \le 1.5SE, \qquad t_{\text{shell}} \ge \frac{PR(\pi^2-8)}{1.5SE(\pi^2-8)-4P} \tag{4}$$

The shell thickness t_{shell} that is greater from Equations (3) and (4) is the minimum requirement.

The stay or center plate is the diffusion bonded core where heat exchange occurs, so typical heat exchanger designers will not have to consider its thickness in their design. Because this project involves designing and testing a header prototype with a plate as a substitute for the core, design requirements are included herein. The total stress shall not exceed SE, therefore requiring that

$$S_{T,\text{plate}} = \frac{2\pi P t_{\text{shell}}^2}{3Rt_{\text{plate}}(\pi^2 - 8)} \leq SE, \qquad t_{plate} \geq \frac{2\pi P t_{\text{shell}}^2}{3R(\pi^2 - 8)SE} \tag{5}$$

Semi-circular headers often have either flat or rounded end caps, the former being more commonly observed in the sCO_2 power cycle field. Flat end cap designs are governed by UG-34 of the BPVC titled "Unstayed Flat Heads and Covers". There are three options for determining the thickness of these end caps. The one included herein is in UG-34(c)(3) that covers flat end caps of many shapes. The required thickness is given by

$$t_{cap} = d\sqrt{\frac{ZCP}{SE}} \tag{6}$$

where d is the "diameter, or short span", $Z = 3.4 - \frac{2.4d}{D}$, D is the "long span of noncircular heads or covers measured perpendicular to short span" d, and $C = 0.2$ according to 13-4(f). Another requirement is that $Z \leq 2.5$. For semi-circular end caps, the short span $d = R$ and the long span $D = 2R$. In this case, $Z = 2.2$ that also satisfies $Z \leq 2.5$ [1]. The resulting thickness requirement is

$$t_{cap} \geq R\sqrt{\frac{0.44P}{SE}} \tag{7}$$

The design requirements also include weld geometry for the welds according to UW-13. There are four types of welds for semi-circular headers: 1) shell-stay, 2) shell-end cap, 3) end cap-stay, and 4) shell-nozzle. The weld detail of the first three can come from Figure UW-13.2(c) of the BPVC [1] while the last can use the ASME Power Piping code B31.1, Figure 127.4.8(a) [5]. The weld requirements of the former typically require the weld to be full penetration that is as wide as it is deep. The weld width at the surface can be twice the material thickness.

HEADER PROTOTYPE DESIGN

The design requirements from the preceding section were used to design a header prototype that was manufactured in triplicate for burst experiments. The prototypes had two semi-circular headers with a single plate between them to simulate the core as well as flat end caps. The stay plate included several large holes for pressure equalization. The design requirements were programmed into a tool in Excel that selects from available pipe and plate material to reduce manufacturing costs. The inputs include P, R, allowable stress S, E, stay plate stress concentration factor K_t, and desired header length. It also considered the design requirements for the four types of welded joints to select thicknesses of the shell, stay, and end cap.

The end caps can either cover the ends of the semi-circular headers or butt up to the inside radius. The former design was selected in this case, but both have been observed in practice. This choice adds a minimum thickness requirement to the end caps and subsequently the stay plate to account for the weld requirements. In practice, the end cap thickness was slightly increased due to weld requirements but the stay plate was significantly increased.

A parameter study was conducted for scaling the header prototype to a pressure typical of sCO_2 power cycles and sizes that were practical for manufacturing, handling, and cost. The resulting design used 4" schedule 160 stainless steel pipe that was 316/316L dual certified for high strength and low carbon content. The pressure rating P was 3.90 ksi (26.9 MPa) where 1 ksi=1000 psi, the allowable stress at room temperature S was 20 ksi (138 MPa), and weld joint efficiency E was 0.70. The resulting shell/pipe thickness t_{shell} is 0.531 inch (1.35 cm), the stay plate thickness t_{stay} is 2.00 inch (5.08 cm), and the end cap thickness t_{cap} is 0.875 inch (2.22 cm). The allowable stresses for all three pieces was the same for dual certified 316/316L and was taken from the ASME BPVC Sec. II-D. The shell/pipe was a seamless pipe product form with specification number SA-376. The stay plate and end caps were a plate product form with specification number SA-240.

The resulting header prototypes are pictured in Figure 3. The nozzles were made from 9/16" high pressure cone and thread tube rated to 60 ksi (414 MPa). This was done so that the nozzles could withstand the high pressures expected at burst without failure. They were manufactured in triplicate so that the burst pressure could be tested with some statistical information on repeatability. While the header designs and manufacturing were completed in line with the BPVC requirements and experienced welders were leveraged, an authorized ASME inspector was not contracted to avoid unnecessary costs in monitoring the fabrication process as would be required for a U-stamped vessel.

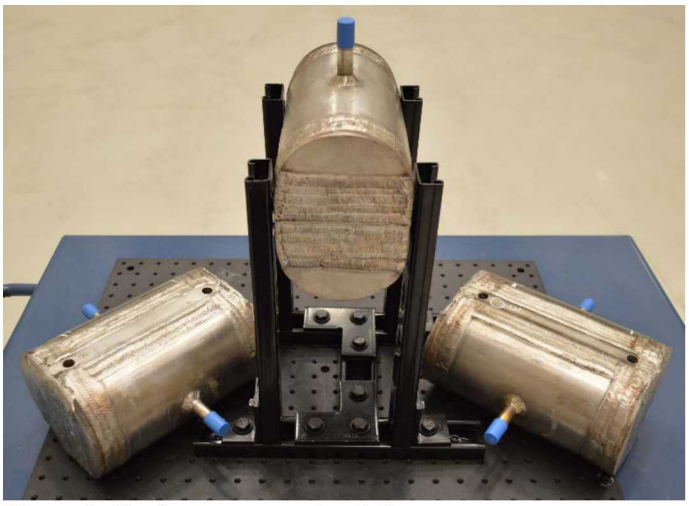

Figure 3, Header prototypes in triplicate

To gain confidence in the weld quality and to investigate for any potential defects, full x-ray inspection was performed on all three prototypes according to the BPVC. An example on Test Article (TA) 1 is shown in Figure 4. All three TAs were free from observable defects. Nevertheless, the weld joint efficiency was assumed 0.7 to remain conservative.

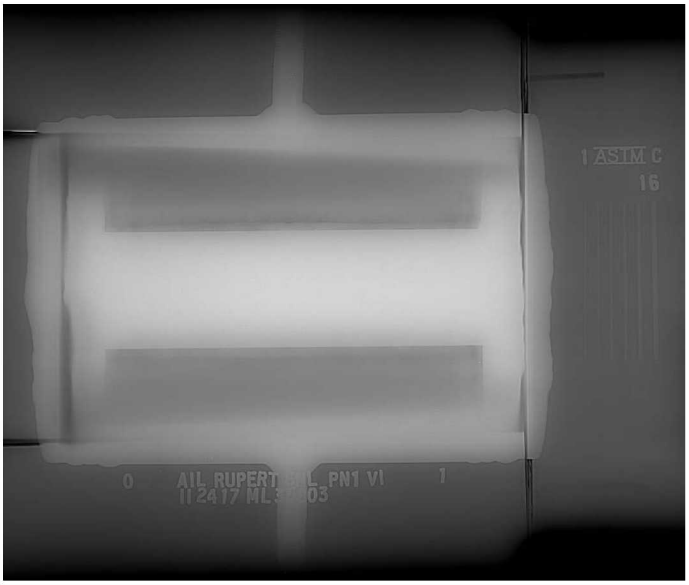

Figure 4, Full x-ray exposure of TA1

HEADER PROTOTYPE BURST EXPERIMENTS

To prepare for these experiments, a custom hydrostatic test cart was procured from Lorimer Corporation to provide pressurization up to 60 ksi (414 MPa) with remote operation capabilities. This allowed the tests to be run inside a shipping container for use as a safety barrier while personnel were located outside. A dedicated National Instruments (NI) data acquisition system was used for system control and data recording. The cart and all associated tube and fittings connecting the cart to the TA were high pressure cone and thread style rated to the cart pressure capacity.

The tests were run with a slow pressure ramp starting with the minimum controllable pressure around 2.5 ksi (17.2 MPa) and increasing until failure. The pressure profiles are shown in Figure 5 for all three TAs. The pressure was held constant at several lower values so that sets of DIC images could be acquired and averaged for the same conditions. The first TA was run manually with a user-specified pressure. Tests for TAs 2 and 3 were run manually for low pressures before starting a linear pressure ramp. The pressure was increased slowly in each case to make sure that the failure was ductile and the burst pressure could be accurately captured. The pressure ramp rates were typically less than 10 psi/s.

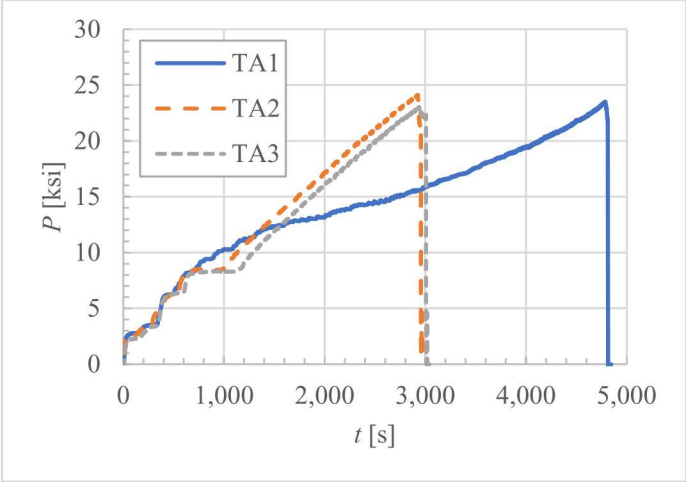

Figure 5, Pressure time histories for all three TAs

The burst pressures are shown in Table 1 with their uncertainties and the pressure safety factors. Systematic uncertainty is presented for each burst pressure and includes that of the pressure transducers and their associated data acquisition module. The uncertainty on the average includes the systematic uncertainties of each reading as well as the random variation in the three samples. Uncertainties were propagated using the Taylor Series Method of Coleman and Steele [6]. The pressure safety factor is $SF = B/P$ where B is the burst pressure and P is the pressure rating of the prototypes under the BPVC.

Table 1, Measured burst pressures for the TAs

TA	Burst Pressure (ksi / MPa)	Uncertainty (ksi / MPa)	Pressure Safety Factor
1	23.50 / 162.0	0.351 / 2.42	6.03
2	24.10 / 166.2	0.353 / 2.43	6.18
3	23.03 / 158.8	0.349 / 2.41	5.91
Ave	23.54 / 162.3	1.37 / 9.45	6.04

The safety factor was measurably higher than the expected value of 4.0. Considering a weld joint efficiency of 1.0 that is justified with full x-ray inspection, the original pressure rating could have been 5.55 ksi. This would result in a pressure safety

factor of 4.24 based on the average pressure, much closer to that expected from the BPVC.

Failures occurred at the nozzle-header weld in all three TAs. Very small holes were formed between the two adjacent weld passes in the fillet weld that led to a very small leak. In post-test inspection, the holes were not visible without magnification. In each case, the pressure dropped by about three ksi while the pump continued to operate and maintain the burst pressure.

The BPVC has provisions for pressure vessel maximum allowable working pressure (MAWP) to be established by burst testing in UG-101. Combining two equations from UG-101(m)(2)(-a) and UG-101(k) and assuming minimum and maximum tensile strength are the same for a given material, the pressure rating is calculated by

$$P = \frac{BE}{4}\frac{S_{\text{DesignTemp}}}{S_{\text{TestTemp}}} \tag{8}$$

where $S_{\text{DesignTemp}}$ is the allowable stress at design temperature and S_{TestTemp} is the allowable stress at test temperature.

Applying Eq. (8) to our header prototype provides a useful verification of the design equations. Since the design used the allowable stress for 316/316L at room temperature, this is considered first. The MAWP at room temperature by the average burst pressure is therefore 4,120 psi, a pressure just 5.6% above the design of 3,900 psi. If we considered the MAWP at an elevated temperature of 550°C (soon before it has a steep reduction with increased temperature) where 316 has an allowable stress of 15.2 ksi (105 MPa), the pressure rating by this burst test is therefore 3,130 psi (21.6 MPa). Even though the welder was not code certified, the pressure rating by burst being very consistent with and higher than the design pressure suggests that the weld quality was sufficient.

FINITE ELEMENT ANALYSIS

Finite Element Analysis was performed on the header prototype design prior to burst testing to predict stress and strain distributions as well as their maximums and associated locations. The geometry was first defined in SolidWorks then imported into the ANSYS environment for meshing and solving. The analysis was performed with ANSYS MECHANICAL 19.1. The mesh used tetrahedral elements that had local refinement near smaller features and corners and is shown in Figure 6. It had 1.09M elements that provided a good balance of spatial resolution and solution efficiency. The internal surfaces had a pressure load applied and one external mounting hole was fixed.

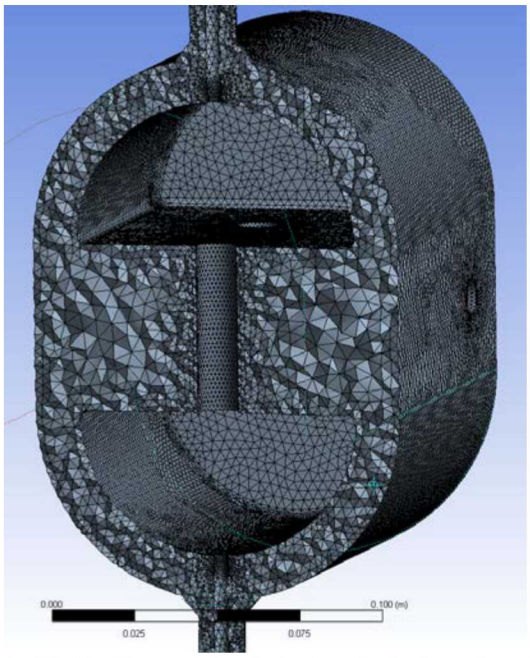

Figure 6, Finite Element Analysis tetrahedral mesh with local refinement

Meaningful pressure values in the FEA model are those for which we have optical strain measurements from DIC. One somewhat near the design pressure is for TA3 at 3410 psi. The predicted stress state is shown in Figure 7 and shows a stress concentration on the inside radius between the stay plate and the end cap. There is also another concentration between the stay plate and the shell, the location of high stress described in the BPVC. Note the deformed state relative to Figure 6 where the center of the headers has elongated. The maximum von-Mises stress is predicted to be 36.7 ksi on the inside corner, higher than the minimum yield strength as defined in the BPVC. This could be a numerical artifact common to FEA where inside corners in tension often show an increase in stress prediction. The stay plate has very low stress as we would expect since it is far oversized to account for the welds on all sides. The end caps have very low stress as well since they are also oversized based on welding requirements.

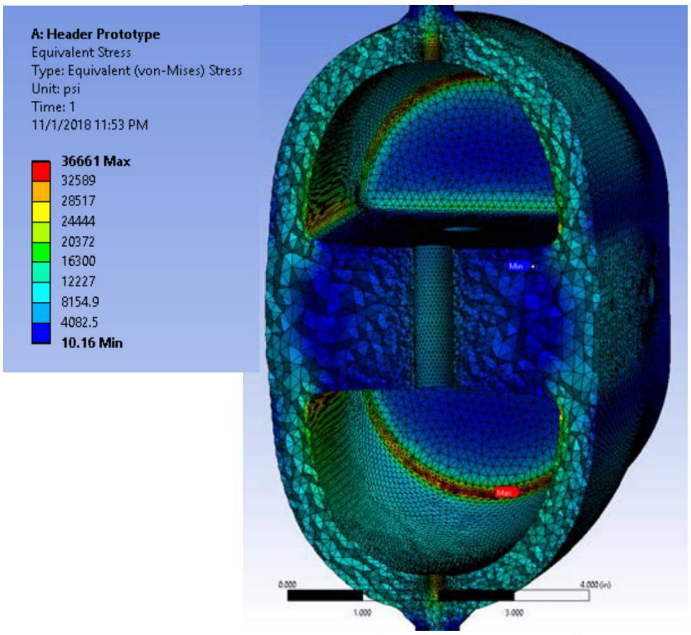

Figure 7, von-Mises stress state in header prototype design

The von-Mises strain on the outer surface is shown in Figure 8 and shows that the semi-circular regions have moderate values. There is a slight peak near the nozzle base with a predicted strain of 560 με. The end caps are even thicker and show very little strain.

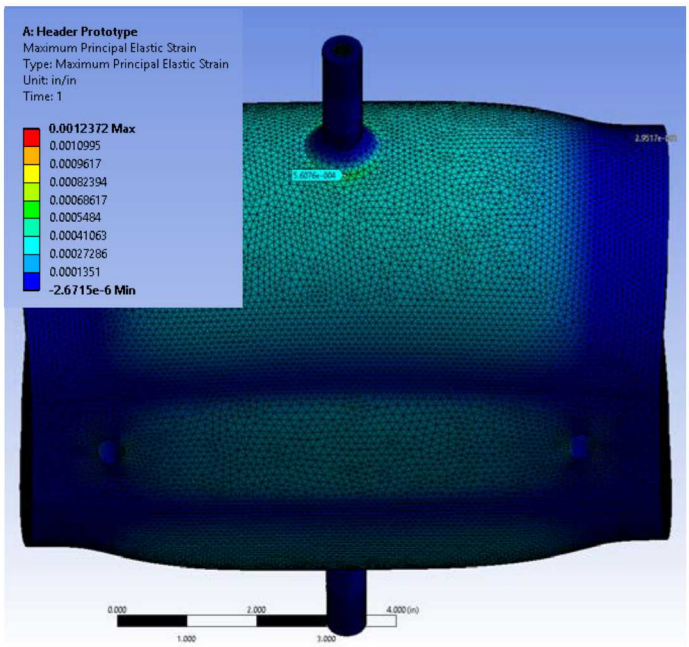

Figure 8, von-Mises strain in header prototype design

Currently the FEA is running the standard elastic strain assumption, so accurate predictions beyond yield are not feasible. The prediction capability will be extended in future revisions of this work by including the stress-strain curve for 316 SS in the materials database. Furthermore, the FEA will be extended to include the pressure ramp measured in experiments for matching of conditions and comparison of FEA and DIC results.

DIGITAL IMAGE CORRELATION

Digital Image Correlation is an optical technique that provides high fidelity strain and deflection measurement results. Compared with strain gages, DIC can provide thousands of strain measurements in two directions on a surface, requires no contact with the TA, is suitable for strains up to approximately 25%, and can measure deflections in space when a stereo configuration is used.

This method requires painting a speckle pattern on the TA to produce a random pattern that has gradients in all directions. The speckle pattern provides information that can be used for tracking displacements. The speckles are imaged first with no strain to use as a reference. Images with strain are then acquired and compared with the reference image over portions of the images that are often tens of pixels square. Each subset has a unique speckle pattern. This pattern is found in the strained images by matching it in the nearby space. Each subset match provides a displacement and deformation. Arrays of displacement can be used together to form a virtual strain gage made up of several subsets.

While a single camera can be used for in-plane strain measurements, there are a lot of advantages to using a stereo configuration with two cameras. The most significant is that out of plane motion can be distinguished with two views while a single camera is not able to distinguish this motion from a uniform strain.

Stereo DIC requires calibration using a target with a known dot pattern. Commercial software can automatically detect the dot pattern in a series of calibration images and can track them as the target is translated and rotated in the field of view. In this experiment, four stereo configurations were used to capture each half of the semi-circular headers. Even though symmetry can be expected across two planes of the prototypes, full coverage was desired to capture strain and defect propagation on any location on the TA. The experimental setup is shown in Figure 9 with the TA and four stereo DIC camera systems. Care was taken to mount the TA and route the plumbing to maintain unrestricted optical access.

Figure 9, Experimental setup with TA in center and DIC cameras surrounding

Strain sensitivity with DIC takes careful attention for low strain values because the noise floor can be high. But with best practices and image averaging when conditions are constant, the noise floor can approach tens of με. In the experiment, low strains were measured for low pressures, thus motivating the need for holding pressure constant as discussed in the experimental section. For low pressures, 100 image sets were acquired and averaged to improve the measurement quality. When pressures and subsequent strains were higher, a linear pressure profile was used as DIC images were acquired at 1 Hz.

Experimental strain measurements are presented for the same pressure as FEA for direct comparisons. A speckle image with von-Mises strain on top is shown in Figure 10 with a similar orientation and color map as in Figure 8. In both, the maximum strain in the view is directly adjacent to the nozzle fillet weld. The FEA prediction is 561 με while the experiment measured 527 με. The same strain trends are also visible such as the low strain on the end caps on the extreme left and right, the low strain near the shell-stay weld with increasing strain on either side. Note that several holes exist in the experimental data where unreliable data were removed.

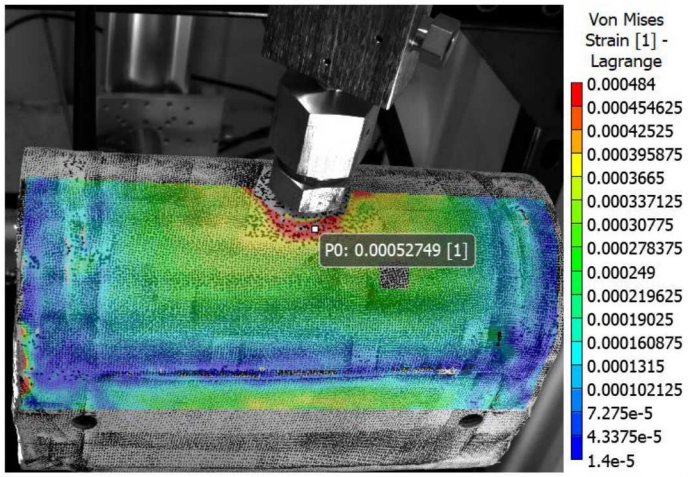

Figure 10, Digital Image Correlation speckle image with superimposed von-Mises strain for near design pressure on TA3

Experimental strain measurements are available from the lowest pressure controllable up to bursting. The strain field for the burst pressure on TA3 of 23.0 ksi is shown in Figure 11 with the strain probe at the same location showing a very large 23.8% strain, equivalent to 238,000 με. This large strain near the nozzle fillet weld is likely what caused the pinhole leaks that appeared on all three TAs. The strain field is different from before as it reaches a maximum near the nozzle attachment and decreases towards both the end caps and the stay plate. The image shows a significant bulging of the shell section of the header when compared with that from Figure 10.

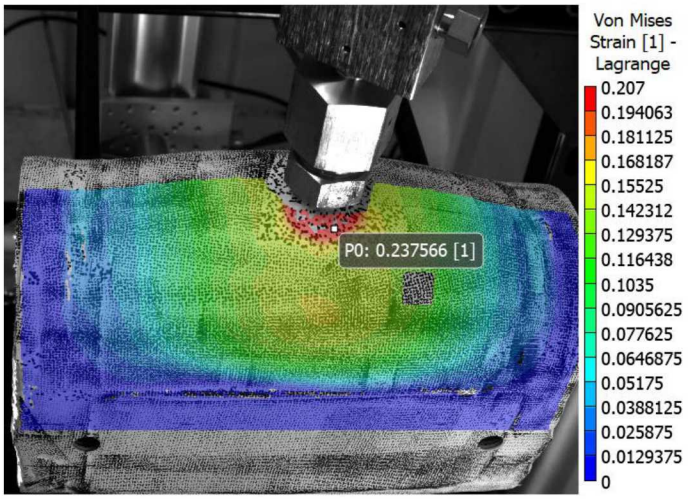

Figure 11, Digital Image Correlation speckle image with superimposed von-Mises strain for burst pressure on TA3

SUMMARY AND CONCLUSIONS

This work is the first known to provide validation testing for the ASME BPVC design by equation for semi-circular headers. The relevant requirements from the code were summarized and applied to the design of header prototypes that were manufactured in triplicate for burst testing. Each was burst while recording pressure and DIC images from four stereo systems.

The measured strain agrees well when comparing trends and the maximum values near the nozzle.

The burst pressures show great consistency and provide a MAWP that is very close to that from the design requirements, giving experimental evidence to the credibility of these equations. The DIC method shows great utility for this and future works in strain measurements, especially in the areas of strain gradients and for high values of strain where traditional gages are not adequate.

NOMENCLATURE

b	Moment of inertia per unit width (1.0)
B	Burst pressure
c	Distance from neutral axis
C	Scaling parameter (0.2 in this work)
d	Diameter or short span
D	Long span of noncircular heads
E	Weld joint efficiency
I	Moment of inertia
K_t	Stress concentration factor
P	Pressure
R	Inside radius of shell
S	Allowable stress
$S_{membrane}$	Membrane stress
S_T	Total stress
S_y	Yield strength
t_{cap}	Thickness of end cap
t_{plate}	Thickness of plate
t_{shell}	Thickness of shell
Z	Scaling parameter

ACKNOWLEDGMENTS

The authors wish to thank the researchers that enabled the DIC aspect of this work, namely Phil Reu and Sam Fayad. The authors also wish to thank the technicians that contributed to the experimental aspect of this work: Rob Sharpe, Ted Sahlstrom, and Arthur Buege.

Sandia National Laboratories is a multimission laboratory managed and operated by National Technology and Engineering Solutions of Sandia, LLC., a wholly owned subsidiary of Honeywell International, Inc., for the U.S. Department of Energy's National Nuclear Security Administration under contract DE-NA-0003525.

REFERENCES

[1] The American Society of Mechanical Engineers, 2017, "2017 ASME Boiler & Pressure Vessel Code," Section VIII, Division 1, New York.

[2] Faupel, J., 1979, "Pressure Vessels of Noncircular Cross Section (Commentary on New Rules for ASME Code)," Journal of Pressure Vessel Technology, 101(3), pp. 255-267.

[3] Castigliano, A., 1879, Théorie de l'équilibre des systèmes élastiques et ses applications, A.F. Negro.

[4] Southwell, R. V., 1923, "On Castigliano's theorem of least work, and the principle of St. Venant," The London, Edinburgh, and Dublin Philosophical Magazine and Journal of Science, 45(265), pp. 193-212.

[5] The American Society of Mechanical Engineers, 2018, "Power Piping B31.1-2018,"New York.

[6] Coleman, H. W., and Steele, G., 2009, Experimentation, Validation, and Uncertainty Analysis for Engineers, John Wiley & Sons, Inc., Hoboken.